JOURNAL OF THE ROYAL SOCIETY Interface

J. R. Soc. Interface (2012) **9**, 3129–3139
doi:10.1098/rsif.2012.0512
Published online 1 August 2012

A dynamical model for the *Utricularia* trap

Coraline Llorens[1], Médéric Argentina[1,*], Yann Bouret[1], Philippe Marmottant[2] and Olivier Vincent[2]

[1]*Université de Nice Sophia Antipolis, LJAD, Faculté des sciences, Parc Valrose, 06100 Nice, France*
[2]*Université Joseph Fourier Grenoble 1, Laboratoire Interdisciplinaire de Physique (CNRS UMR 5588), BP 87, 38402 St Martin D'Hères, France*

We propose a model that captures the dynamics of a carnivorous plant, *Utricularia inflata*. This plant possesses tiny traps for capturing small aquatic animals. Glands pump water out of the trap, yielding a negative pressure difference between the plant and its surroundings. The trap door is set into a meta-stable state and opens quickly as an extra pressure is generated by the displacement of a potential prey. As the door opens, the pressure difference sucks the animal into the trap. We write an ODE model that captures all the physics at play. We show that the dynamics of the plant is quite similar to neuronal dynamics and we analyse the effect of a white noise on the dynamics of the trap.

Keywords: bladderwort; carnivorous plant; fast motion; excitable dynamics; *Utricularia*

1. INTRODUCTION

Utricularia inflata is an amazing, aquatic, rootless plant. At first sight, they are long stems topped by yellow flowers, but their underwater leaves are endowed with millimetre-sized traps. These traps are ingenious systems developed by the plant in order to survive in nutrient-poor habitats. When a prey comes too close to the trap, it touches some trigger hairs (figure 1*a*). This mechanical stimulus allows the opening of the trap: the door buckles, slides inwards and finally unlocks. Thus, the prey and its surrounding water are quickly sucked into the inflating trap (figure 1*c*). Then, *Utricularia* deflates slowly, thanks to the activity of membranar bifid glands, which actively pump the water out of the trap. Actually, the pumping is based on the transport of chloride ions, which creates a local osmotic gradient in the trap membrane and an accompanying flux of water [1,2]. As a result, the trap deflates and returns into a capturing configuration (figure 1*b*).

In order to fully understand the mechanical behaviour of this trap, we built a full dynamical model. Indeed, previous studies focus only on the mechanics of the trap body [3], or on the door [4] but no model was proposed to link those two aspects. Here, we introduce the hydrodynamics in order to couple these two elastic parts. We present our model in §2 by linking the internal pressure and the position of the door with a set of two coupled differential equations. Our dynamical model predicts a wide range of behaviours, including excitability leading to a fast suction, and spontaneous or periodic firings, which are all observed experimentally on *Utricularia* [5]. Note that our purely *mechanical* system is described by a set of equations that are similar to that of other models developed for electrically excitable media, such as the FitzHugh–Nagumo model for spike generation in nerves [6]. We find the relevant parameters that completely characterize the whole dynamics. Numerical results are analysed in §3. In §4, we discuss the suitability of our model by comparing our results with the real behaviour of *Utricularia*. Fluctuations are introduced in the last section, in order to account for the statistics of spontaneous firings of the trap [5].

2. DERIVATION OF THE MODEL

The mechanism for capturing prey is based on the suction of the fluid near the door, induced by the trap deformation. The bifid glands, by expelling water, build up a high pressure difference between the interior and the exterior of the trap, with a characteristic time of a hundred minutes. For a critical volume, the closed door can no longer sustain this pressure difference, and the trap inflates in a few milliseconds while sucking in the exterior fluid (with the potential prey). The existence of a critical threshold yielding an explosive response followed by a slow recovery are the signature of an excitable system, like for the neuronal dynamics [6].

We first describe the geometric properties of the trap, then we model the temporal variations of the volume and we approximate the door opening/closing dynamics. Finally, we close our model by coupling this dynamics with the volume equation.

*Author for correspondence (mederic.argentina@unice.fr).

Received 28 June 2012
Accepted 6 July 2012

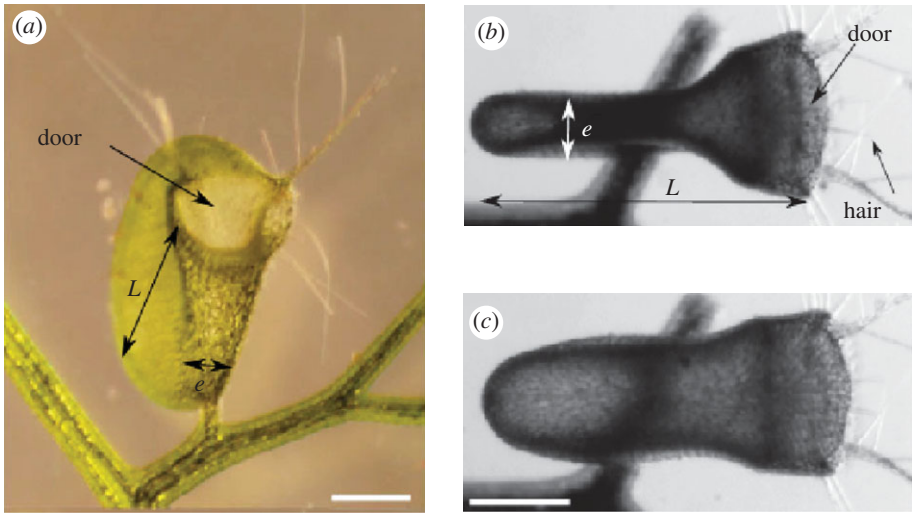

Figure 1. Trap of *Utricularia inflata*. (*a*) Frontal view of the trap. The light green disc is the door of the trap. (*b*,*c*) Top view of a trap. The two extreme states of the trap are displayed. In (*b*), the trap is in the deflated, capturing configuration. The fine threads are the trigger hairs. In (*c*), the trap has just fired and is inflated. Scale bars, 500 µm. (Online version in colour.)

2.1. Geometry of the trap body

The trap, which is a biconcave disc, as pictured in figures 1 and 2, can be approximated as a deformable cylinder [4] of diameter $L \approx 1.5$ mm and variable height e. The volume is approximated by

$$V = \pi \left(\frac{L}{2}\right)^2 e. \tag{2.1}$$

When the trap is fully inflated, $e = 0.8$ mm, and the maximum volume is $V_{\max} = 1.41\ \text{mm}^3$. As the trap is fully deflated, $e = 0.4$ mm, and the minimal volume is $V_{\min} = 0.67\ \text{mm}^3$ [4]. The area of the membrane of the trap S_m is approximately given by

$$S_\text{m} = \frac{\pi}{2} L^2 + \pi L e. \tag{2.2}$$

2.2. Temporal variation of the volume

We now consider the temporal variations of V, as observed in [5]. Experiments show that V decays exponentially to a final volume V_0 [4]. The fluid flux has three contributions. First, the bifid glands of the membrane actively pump the water out of the trap to decrease V. The flow rate corresponding to this mechanism is $-q$ with q positive. The second effect is related to the porosity of the trap. The membrane pores induce a Darcy flow that is proportional to the pressure difference ΔP, the surface of the membrane S_m and the porosity δ_e. Osmotic pressure could also be at the origin of this leakage. Finally, if the door is opened, there is an additional flux that tends to equilibrate the pressure difference between the exterior and the interior of the trap. For now, we simply write the balance of fluxes related to the membrane:

$$\frac{\partial V}{\partial t} = -q + \delta_\text{e} S_\text{m} \Delta P, \tag{2.3}$$

where $q = 2.3 \times 10^{-13}\ \text{m}^3\,\text{s}^{-1}$ [4] (equivalent to a transport velocity of $4 \times 10^{-8}\ \text{m}\,\text{s}^{-1}$ through the surface

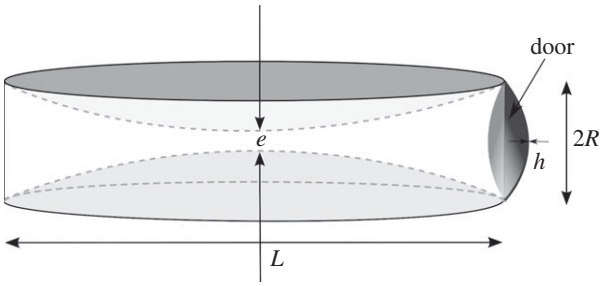

Figure 2. Cylindrical geometry of the trap, with a diameter L and a height e. The door is visible on the right as a circular shell of radius R ($R = 3 \times 10^{-4}$ m) and thickness h ($h = 3 \times 10^{-5}$ m) [3].

S_m) and we choose $\delta_\text{e} = 2.4 \times 10^{-12}\ \text{m}\,\text{s}^{-1}\,\text{Pa}^{-1}$ of the same order of magnitude as those reported for vegetal cells [7,8]. The membrane elasticity connects the volume loss to the pressure load: the pressure difference ΔP varies almost linearly with V in experiments and in simulations [4]:

$$\Delta P = -d(V - V_{\max}), \tag{2.4}$$

with $V_{\max}$ the volume for which the bending energy of the trap is minimum. Here, d mixes the effects of the elasticity and the geometry of the trap. Experimental results show that a variation from $V = V_{\max}$ to $V = V_{\min}$ yields a pressure difference equal to 0.15 bar [4]; so we evaluate $d = 2.027 \times 10^{13}\ \text{Pa}\,\text{m}^{-3}$. As a consequence, we conclude from (2.3) and (2.4):

$$\dot{V} = \frac{1}{\tau}(V_0 - V), \tag{2.5}$$

where $1/\tau = \delta_\text{e}\, d S_\text{m}$ and $V_0 = V_{\max} - q\tau$ is the volume at final equilibrium.

At this stage, we can model the action of the door with the following argument: as V becomes smaller than V_c, the door opens and V is settled instantly to a given value $V_{\max}$. This crude approximation

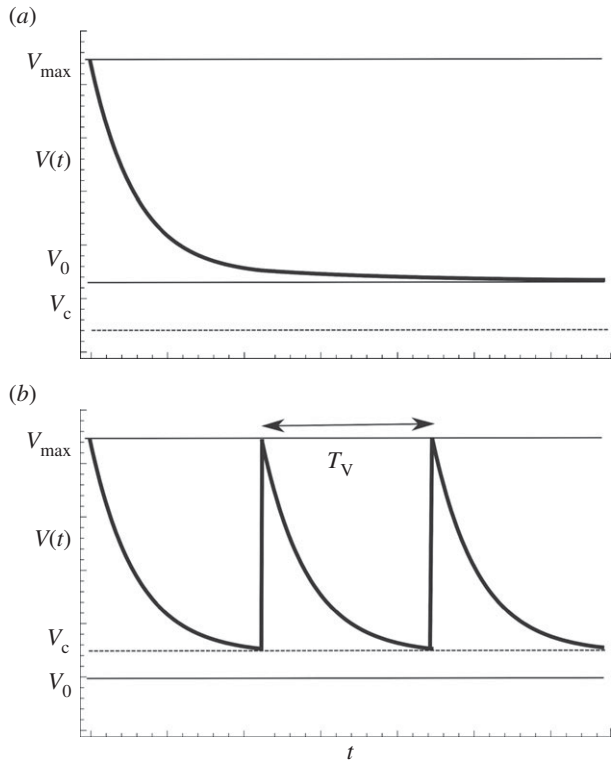

Figure 3. Temporal variations of the volume V, with a simple model neglecting the door dynamics. (*a*) $V_c < V_0$: convergence of the trap volume to V_0. (*b*) $V_c > V_0$: oscillations of the volume V.

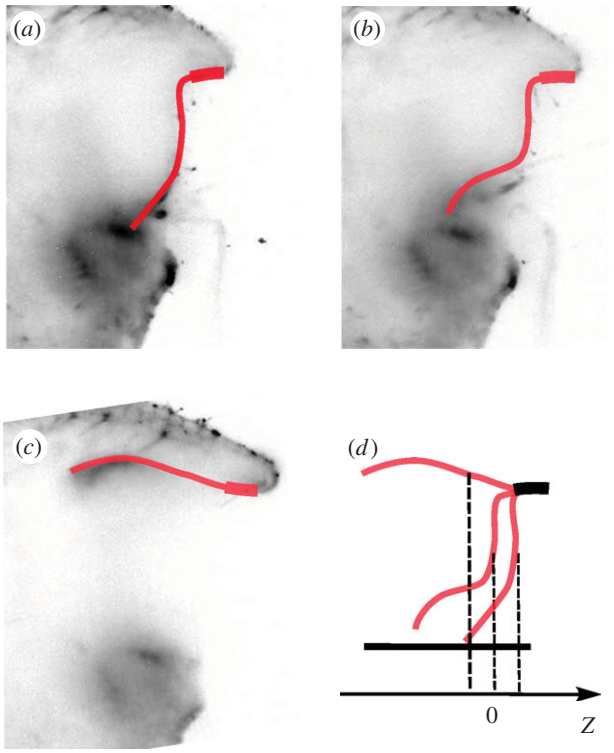

Figure 4. Experimental images of the opening of the door of *Utricularia australis*. (*a*) Initial shape prior opening, (*b*) 7.6 ms after opening and (*c*) full opening at 8.6 ms. The height of the door is around 400 µm. It is thicker near top. The pictures are based on light-sheet fluorescence microscopy recording and they are here displayed in grey inversion. (*d*) The conventions for the position of the centre of the door Z are represented. When the door is closed and the trap is in the 'ready to capture' configuration, $Z = +Z_0$. The door is buckling: $Z = 0$. The curvature of the door is inverted and the door is open: $Z = -Z_0$. (Online version in colour.)

will be refined as we develop the model of the door displacement (§2.3).

If at $t = 0$, $V = V_{max}$, then the temporal evolution of the volume is

$$V(t) = V_0 + (V_{max} - V_0)\, e^{-t/\tau}. \tag{2.6}$$

Consequently, depending on the relative value of V_0 to V_c, we can observe two distinct behaviours (figure 3):

— if $V_c < V_0$, the volume of the trap converges to V_0. Furthermore, if $V_c \sim V_0$, the trap dynamics is similar to an excitable system [9]. A small external perturbation can potentially decrease V under V_c, leading to the opening of the door, which in turn increases V up to V_{max}.

— if $V_c > V_0$, the volume will oscillate between the value V_{max} and V_c. The period of the oscillation T_V can be easily obtained. At $t = T_V$, the door opens as $V = V_c$. We therefore deduce from (2.6) that

$$T_V = \tau \log \frac{V_{max} - V_0}{V_c - V_0}. \tag{2.7}$$

These two distinct behaviours have been described in Vincent *et al.* [5].

The critical volume V_c will be assessed by studying the door dynamics.

2.3. Dynamics of the door

We model the door as an elastic circular shell of radius $R = 3 \times 10^{-4}$ m and thickness $h = 3 \times 10^{-5}$ m [4], with half of its edge clamped in the membrane. This door is compressed against a flat and rigid substrate, leading to a bent shape as pictured in figure 4*a*. In this configuration, we assume that no fluid leaks through the door, which slightly deforms to sustain an increase in pressure difference ΔP. When this latter exceeds a critical value, a buckling instability occurs (figure 4*b*), yielding to a fast opening of the door that permits a fast entrance of the fluid that equilibrates the pressure (figure 4*c*). Once ΔP vanishes, the door comes back quickly to its original configuration (figure 4*a*), driven by the minimization of its elastic energy.

We note Z the position of the centre of mass of the door. The door is subject to elastic forces, to the external load $-\pi R^2 \Delta P$ exerted by the pressure and to damping. The effective mass m of the door can be approximated by

$$m = \rho \pi R^2 h + \kappa \rho R^3, \tag{2.8}$$

where ρ measures its density (approx. equal to $\rho_{water} = 10^3$ kg m^{-3}). The first term is the mass of the door, and the second term represents the added mass. The factor

κ is of order 1 [10]. The cubic dependance models the fluid volume that the door needs to displace during its motion. We consequently write:

$$m\ddot{Z} = f_{\text{elastic}} + f_{\text{damping}} - \pi R^2 \Delta P. \tag{2.9}$$

Very roughly, the damping terms can be written with a sum of two contributions. As the door moves fast, the fluid is at a high Reynolds number and generates a drag proportional to $\rho(\dot{Z})^2$ [11]. For small movements, the latter damping is small compared with the viscous friction, proportional to the Stokes force $\eta R\dot{Z}$ [11], where η is the dynamical viscosity of water. Consequently, we write:

$$f_{\text{damping}} = -a\rho R^2(\dot{Z})^2 \text{sign}(\dot{Z}) - b\eta R\dot{Z}, \tag{2.10}$$

where the two constants a and b are of order 1, and depends on the geometry of the door. It remains to define the elastic forces. We approximate the door with a cylindrical shell, against a rigid substrate using a bending energy $\mathcal{E}$:

$$f_{\text{elastic}} = -\frac{\partial \mathcal{E}}{\partial Z}. \tag{2.11}$$

For such systems, the plate has two stable buckled equilibria separated by an unstable state. The bending energy should display two minima separated by one maximum, this is why we propose

$$\mathcal{E} = -P_{\text{b}} R \frac{Z^2}{2}\left(1 - \frac{1}{2}\left(\frac{Z}{Z_0}\right)^2\right), \tag{2.12}$$

where P_{b} is the critical pressure provoking the door buckling. In the case of a spherical shell of radius R and thickness h, it writes $P_{\text{b}} = Eh^2/R^2$ [12].

The energy (2.12) predicts an unstable state $Z = 0$ with two stable states $Z = \pm Z_0$. Following figure 4, we choose the door to be closed when $Z > 0$ and opened when $Z < 0$. The door is not articulated on freely rotating hinges, as would be a real door. Actually, it is clamped to the main body by a thicker and less deformable part (figure 4). The deformation of this thicker part means that the opened state is energetically unfavoured. To account for the deformation cost of the thick part, we therefore break the symmetry $Z \to -Z$ by adding a term proportional to $-Z$ in the energy and we introduce a prefactor c:

$$\mathcal{E} = -P_{\text{b}} R\left[\frac{Z^2}{2}\left(1 - \frac{1}{2}\left(\frac{Z}{Z_0}\right)^2\right) + cZ_0 Z\right]. \tag{2.13}$$

In figure 5, we plot the elastic energy $\mathcal{E}$ as a function of Z. The effect of the constant $c > 0$ renders the closed door configuration to be more stable from an energetic point of view. In particular, when $c > 2/3\sqrt{3}$, this potential exhibits a single minimum, with $Z > 0$, which corresponds to the closed door state.

2.4. Mass flux induced by the door

It remains to couple the volume equation (2.6) to the door dynamics (2.9). We model the flow rate Q in the channel induced by the opened door, in the presence of a pressure difference:

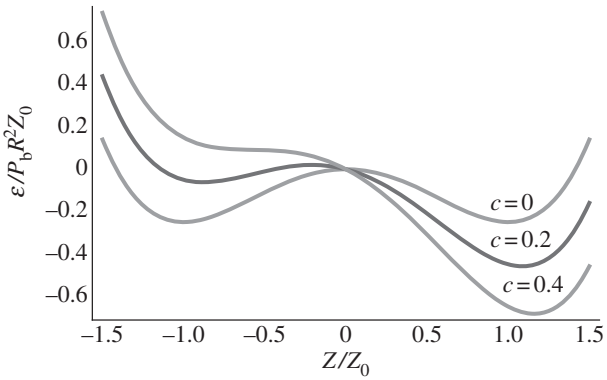

Figure 5. $\mathcal{E}$ versus Z for $c = 0$, 0.2, 0.4.

$$Q = \pi R^2 s\left(\frac{Z}{Z_0}\right) U. \tag{2.14}$$

Here, $\pi R^2 s(Z/Z_0)$ is the surface of the channel. The non-dimensional surface $s(Z/Z_0)$ is approximated with

$$s(x) = -fx\mathcal{H}(-x), \tag{2.15}$$

where $\mathcal{H}(x)$ is the unit step function. The constant f is a geometric factor.

The fluid velocity U can be assessed using Bernouilli relation [11], because the Reynolds number of the incoming flow is quite high (around 1000 [3]). We therefore write

$$U = \text{sign}(\Delta P)\sqrt{\frac{2}{\rho}|\Delta P|}. \tag{2.16}$$

As consequence, we deduce the flux Q

$$Q = \text{sign}(\Delta P)\pi R^2 \sqrt{\frac{2}{\rho}|\Delta P|}\, s\left(\frac{Z}{Z_0}\right). \tag{2.17}$$

2.5. Model closure

In order to close the model, we need to couple the volume, the door position and the pressure difference. Adding the contribution of the open door (2.17) to the flux balance (2.3), we obtain

$$\frac{\partial V}{\partial t} = -q + \delta_{\text{e}} S_{\text{m}} \Delta P + \text{sign}(\Delta P)\pi R^2 \sqrt{\frac{2}{\rho}|\Delta P|}\, s\left(\frac{Z}{Z_0}\right). \tag{2.18}$$

Injecting the link (2.4) between ΔP and V into the earlier-mentioned relation, we deduce our dynamical model for the trap:

$$\Delta P = -d\left[-q + \delta_{\text{e}} S_{\text{m}} \Delta P + \text{sign}(\Delta P)\pi R^2 \sqrt{\frac{2}{\rho}|\Delta P|}\, s\left(\frac{Z}{Z_0}\right)\right] \tag{2.19}$$

and

$$m\ddot{Z} = P_b R\left(Z - \left(\frac{Z}{Z_0}\right)^2 Z + cZ_0\right) - \pi R^2 \Delta P - a\rho R^2(\dot{Z})^2 \mathrm{sign}(\dot{Z}) - b\eta R\dot{Z}. \quad (2.20)$$

We now set our system in a non-dimensional form with the scalings $Z = Z_0 z$, $\Delta P = P_b p$, and $t = \Theta s$. Because the characteristic length scale for Z_0 is proportional to R, we set $Z_0 = R$. Using (2.20), the balance between the acceleration term with the elastic response gives the characteristic timescale Θ of the opening door:

$$\Theta = \sqrt{\frac{m}{P_b R}} \sim 100\,\mu\mathrm{s}, \quad (2.21)$$

where we used $E = 2.7$ MPa. Θ is the shortest time of the system; so the non-dimensional time s is very long. As consequence, our non-dimensional system can be written as

$$\ddot{z} + \alpha\,\dot{z}^2\,\mathrm{sign}(\dot{z}) + \beta\dot{z} = z - z^3 + c - \lambda p \quad (2.22)$$

and

$$\dot{p} = \frac{1}{\tau_p}(p_0 - p) - \mathrm{sign}(p)\gamma\sqrt{|p|}s(z), \quad (2.23)$$

with

$$\alpha = a\frac{\rho Z_0 R^2}{m} \sim 0.34, \quad (2.24)$$

$$\beta = b\frac{\eta R\Theta}{m} \sim 3.7 \times 10^{-4}, \quad (2.25)$$

$$\gamma = \Theta d\pi R^2\sqrt{\frac{2}{\rho P_b}} \sim 0.16, \quad (2.26)$$

$$\lambda = \frac{\pi R}{Z_0} = \pi, \quad (2.27)$$

$$p_0 = \frac{q}{\delta_e S_m P_b} \sim 0.56 \quad (2.28)$$

and

$$\tau_p = \frac{1}{\Theta d\delta_e S_m} \sim 3.2 \times 10^7. \quad (2.29)$$

The dynamical viscosity is $\eta = 10^{-3}$ Pa s.

3. ANALYSIS OF THE MODEL

The system (2.22) and (2.23) presents two very different timescales. The door motion is generally very fast compared with the pressure recovery time: it is reminiscent of excitable system, for which a qualitative analysis is performed using nullclines. Owing to the slow temporal variation of p, the equation (2.22) is a nonlinear, damped oscillator for the variable z. When $\dot{z} = 0$, the door accelerates positively if $\pi p < f(z)$, with $f(z) = z - z^3 + c$, and negatively otherwise.

If $z > 0$, the equation (2.23) is

$$\dot{p} = \frac{1}{\tau_p}(p_0 - p), \quad (3.1)$$

and the pressure increases as $p_0 > p$, and decreases on the other case.

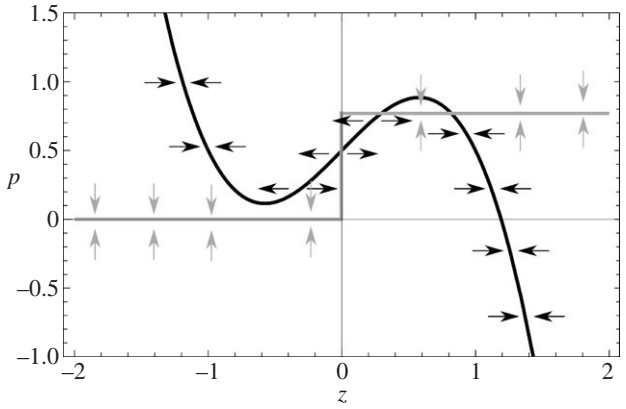

Figure 6. Nullclines for the vector field (z, p). The black curve represents stationary points for which $\ddot{z} = \dot{z} = 0$, i.e. $p = f(z)$, the grey curve represents the location where $\dot{p} = 0$.

If $z < 0$, the door is opened and the fluid flow (through the opening) controls the pressure variation; the equation (2.23) becomes

$$\dot{p} = -\mathrm{sign}(p)\gamma\sqrt{|p|}s(z). \quad (3.2)$$

In consequence, if $z < 0$ and $p > 0$, the pressure difference p decreases whereas if $z < 0$ and $p < 0$, p increases. These behaviours can be summarized in figure 6, where we plot the functions $p(z)$ at which $\dot{p} = 0$ and $\dot{z} = 0$, defining the two nullclines.

The temporal evolution of p is very small compared with z, except in the close neighbourhood of $p = (z - z^3 + c)/\pi$.

3.1. Stationary states

In this section, we investigate the stationary states (z_s, p_s) of the model, and we need to solve the following system of equations:

$$\frac{1}{\tau_p}(p_0 - p_s) - \mathrm{sign}(p_s)\gamma\sqrt{|p_s|}s(z_s) = 0 \quad (3.3)$$

and

$$\frac{z_s - z_s^3 + c}{\pi} = p_s. \quad (3.4)$$

They can be guessed by studying the intersections of the two curves plotted in figure 6. Because the temporal evolution of p is very small compared with those of z, we can assess the linear stability of the fixed points by using the equation (2.22) with $p = p_s$; then the evolution of the perturbation $\tilde{z}$ around z_s obeys to

$$\dddot{\tilde{z}} + \beta\ddot{\tilde{z}} = f'(z_s)\tilde{z}. \quad (3.5)$$

As a consequence, the stationary points z_s will be stable if $f'(z_s) < 0$, because β is always positive.

Depending on the signs of z_s and p_s, we meet two cases:

— $z_s > 0$, the fixed points are $p_s = p_0$ (from (3.1)) and the roots z_s of $\pi p_0 = z_s - z_s^3 + c$. This last equation has two real solutions if $c < \pi p_0 < c + 2/3\sqrt{3}$. A close look at figure 6 permits us to conclude that only the highest root is stable. If $p_0 < c/\pi$,

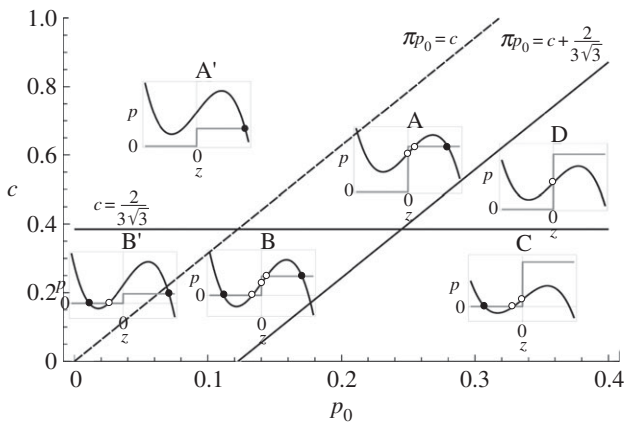

Figure 7. A phase diagram of the dynamical model as a function of the two controlling parameters (p_0, c). The lines separate the different behaviours that the trap can exhibit. The insets represent the nullclines in the (z, p) plane, where the black discs mark a stable stationary point, whereas the white discs represent unstable points. See the main text for the description of each region.

then the system has only one stable stationary point. Perturbations of the door position around these stable states will create damped oscillations, while p will decrease very slowly to p_0.

— $z_s < 0$: in such a case, the flow through the door dominates the dynamics for the pressure. Therefore, $p_s = 0$ (from equation (3.2)). It is necessary to solve $z_s - z_s^3 + c = 0$, which admits two real negative solutions only if $c < 2/3\sqrt{3}$. Again, figure 6 predicts that only the most negative root will be stable.

3.2. Phase diagram

The previous study of stationary states and their linear stability yields the construction of the phase diagram of the trap. Depending on the number of stable states, we distinguish four regions (figure 7):

— Region A and A′: the only stable state is the closed door. Notice that when the pumping generates a pressure difference close to spontaneous buckling, i.e. when $\pi p_0 \lesssim c + 2/3\sqrt{3}$, the system will exhibit a strong sensibility to a variation of the pressure or to the position of the door. It is in this regime that the system is understood as excitable. We made a simulation of the dynamics in this case, as shown in figure 8: a small increment of pressure will lead to a quick opening of the door, producing damped oscillations while it comes back to the closed state, and that the bifids glands pump the fluid out. The pressure difference equilibrates to p_0, and the trap will be ready to capture another prey.

— Region B and B′: in this range of parameters, the trap has two stable steady states: depending on initial conditions, the door remains opened or closed. An example of these dynamics is shown in figure 9.

— Region C: the only stable state is the door opened. An example of these dynamics is shown in figure 10.

— Region D: because the trap does not offer stable stationary points, it undergoes relaxation oscillations between $\pi p_{\min} = f(-1/\sqrt{3}) = c - 2/3\sqrt{3}$ and $\pi p_{\max} = f(1/\sqrt{3}) = c + 2/3\sqrt{3}$. An example of these dynamics is shown in figure 11.

4. DISCUSSION

4.1. Comparison with experiments

Experimentally, the trap presents the three states: excitable, metronomic and dead, described in §3. If the plant is dead, the trap is not functioning anymore, and the trap remains opened as shown in the region C of figure 7. In normal conditions, the trap is in state A of figure 7, with $\pi p_0 \lesssim c + 2/3\sqrt{3}$: a small amount of extra pressure can force the door to open, yielding the suction of some liquid around it. For the simulations presented in figure 12, the variation in pressure difference rises to approximately 16 kPa,with the parameter values proposed in §2.5. This perfectly agrees with the experimental value of 10–20 kPa [4]. The duration for the trap to come back to its stable state is evaluated by $\tau \sim 54$ min, which fairly matches the experimental values of 25–50 min [5]. Finally, we numerically find (figure 10) that the time for the door buckling is around 3.6 ms, namely in the same order of magnitude as those reported in Vincent *et al.* [5].

Obviously, our simple model does not pretend to be accurate enough to exactly match the experiments; however, our non-dimensional parameters can be fit to experimental measures. The model shows that the trapping function is obtained only in one regime, when the mechanical parameters of the trap are in a specific range.

4.2. Effect of noise on the system

This highly sensitive trigger renders the mechanism for capturing preys very efficient; nevertheless, we shall investigate the effect of noise. In fact, for high enough amplitudes, some noise induces stochastic trapping events because of the excitable behaviour.

The relaxation oscillations observed in the D region of the phase diagram have been recently described as spontaneous firings [5]. To investigate the effect of the noise, we consider the membrane as N interconnected 'particles' submitted to an external noise. Accordingly, the positions of the particles follow the Langevin equations:

$$\forall 1 \le j \le N, \partial_t \boldsymbol{r}_j = \frac{D_L}{k_b T} \boldsymbol{f}_j + \boldsymbol{\eta}_{bj}, \tag{4.1}$$

where D_L is the diffusion coefficient, k_b is the Boltzmann constant, T is the temperature, $\boldsymbol{f}_j$ is the external force on the jth particle. The Gaussian random drifts are defined by

$$\left.\begin{aligned} \langle \boldsymbol{\eta}_{bj}(t) \rangle &= \boldsymbol{0} \\ \text{and} \qquad \langle \boldsymbol{\eta}_{bj}(t)\, \boldsymbol{\eta}_{bj}(t') \rangle &= 2D_L \delta(t - t'). \end{aligned}\right\} \tag{4.2}$$

This description allows us to access the stochastic fluctuations of the volume V (see appendix A for details):

$$\dot{V} = \frac{1}{\tau}(V_0 - V) + \Lambda_m(t), \tag{4.3}$$

where $1/\tau = \delta_e \, dS_m$ and $V_0 = V_{\max} - q\tau$ is the trap volume at equilibrium. The stochastic forcing for the

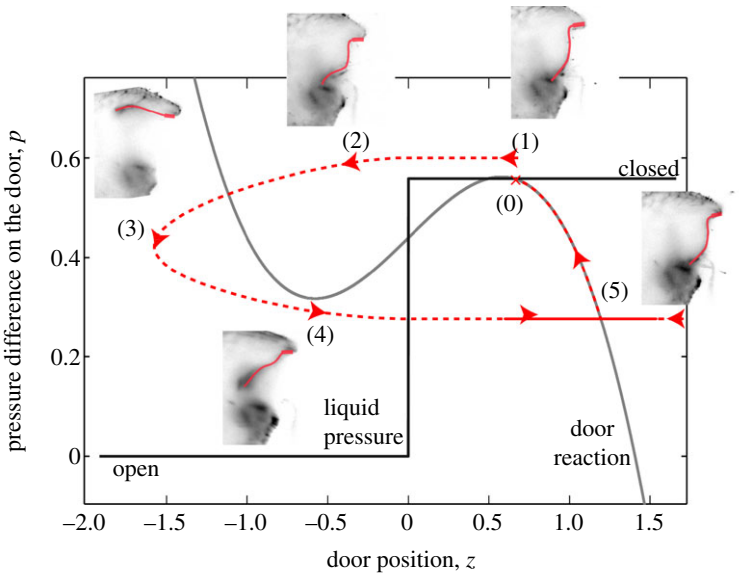

Figure 8. Dynamical evolution of a trap that is near spontaneous buckling: (0) rest position. (1) A mechanical disturbance is added, as a consequence of a prey touching a trigger hair, elevating the pressure difference above buckling threshold, (2) the door is thus opening and (3) is fully opened, so that the pressure difference decreases. (4) Owing to its elasticity, the door closes back; after some oscillations, (5) the pressure difference slowly rises again because of active pumping of fluid, recovering the equilibrium position (0). These results are computed for region A with the following parameters $c = 1.38$ and $p_0 = 0.5581$ and initial conditions: $z = 1, \dot{z} = 0$, $p = 0$ and $v = 1$. (Online version in colour.)

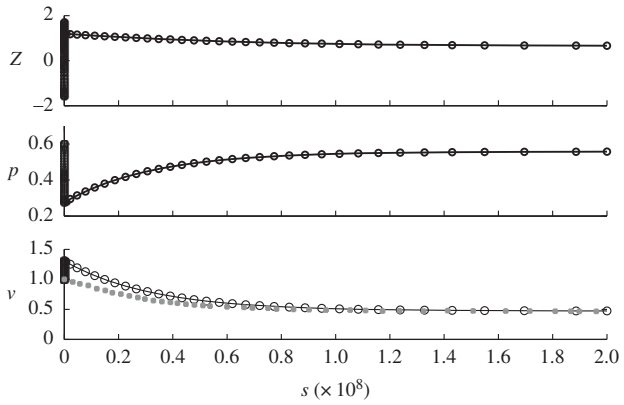

Figure 9. Results for region A, with the time evolution of the normalized door position, pressure and volume. Parameters are same as those of the previous figure. Experimental points for the evolution of the volume are added: v_{exp}. Circles, v; squares, v_{exp} [4].

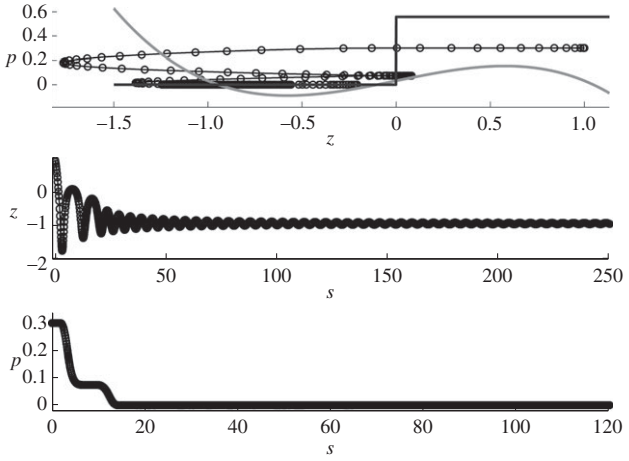

Figure 10. Results for region C with the following parameters $c = 0.1$ and $p_0 = 0.5581$, and initial conditions: $z = 1$, $\dot{z} = 0$, $p = 0.3$ and $v = 1$. Note that the timescale is zoomed in order to see the fast variations. The behaviour remains the same at long timescale: no more variation.

volume is defined by

$$\left.\begin{aligned} &\langle \Lambda_m(t)\rangle = 0 \\ \text{and}\quad &\langle \Lambda_m(t)\Lambda_m(t')\rangle = 2\phi D_{\mathrm{L}}\delta(t-t'), \end{aligned}\right\} \tag{4.4}$$

where ϕD_{L} is a macroscopic volume diffusion coefficient computed in appendix A.

We need to compute the minimum volume V_{c} that the trap can sustain, corresponding to the highest pressure difference ΔP_{c} that the system can maintain:

$$\Delta P_{\mathrm{c}} = \frac{P_{\mathrm{b}}}{\pi}\left(c + \frac{2}{3\sqrt{3}}\right). \tag{4.5}$$

The critical volume is straightforwardly deduced from the relation (2.4):

$$V_{\mathrm{c}} = V_{\max} - \frac{\Delta P_{\mathrm{c}}}{d}. \tag{4.6}$$

If $V < V_{\mathrm{c}}$, the doors opens and the trap volume instantaneously reaches $V_{\max}$.

We translate (4.3) with the following change of variable:

$$x = \frac{V - V_{\mathrm{c}}}{V_{\max} - V_{\mathrm{c}}}, \tag{4.7}$$

$$x_0 = \frac{V_0 - V_{\mathrm{c}}}{V_{\max} - V_{\mathrm{c}}} \tag{4.8}$$

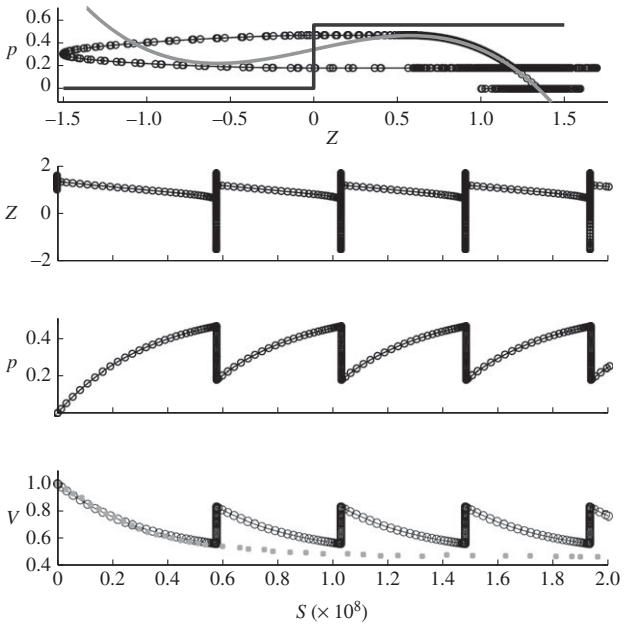

Figure 11. Results for region D with the following parameters $c = 1.0733$ and $p_0 = 0.5581$ and initial conditions: $z = 1$, $\dot{z} = 0$, $p = 0$ and $v = 1$. Circles, v; squares, v_{exp}.

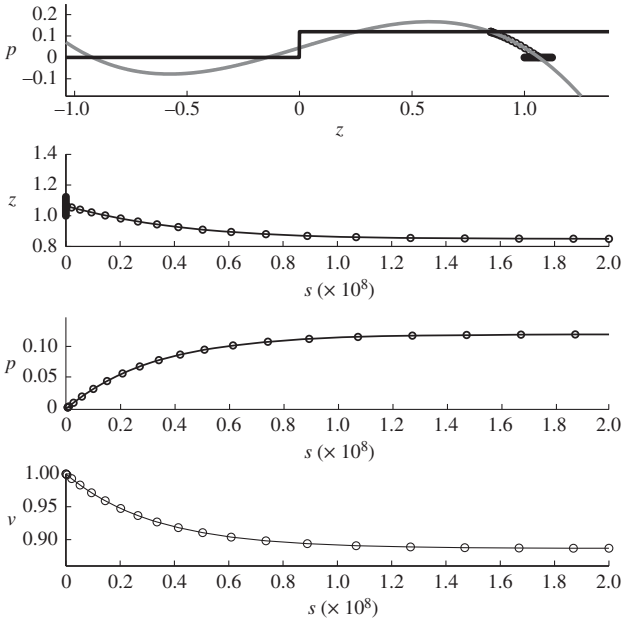

Figure 12. Results for region B with the following parameters $c = 0.14$ and $p_0 = 0.12$, and initial conditions: $z = 1$, $\dot{z} = 0$, $p = 0$ and $v = 1$.

and
$$x_{\max} = \frac{V_{\max} - V_{\mathrm{c}}}{V_{\max} - V_{\mathrm{c}}} = 1. \tag{4.9}$$

Then, (4.3) becomes:

$$\dot{x} = \frac{1}{\tau}(x_0 - x) + \Lambda(t), \tag{4.10}$$

with
$$\Lambda(t) = \frac{\Lambda_m}{V_{\max} - V_{\mathrm{c}}}. \tag{4.11}$$

Depending on the sign of x_0, the trap can exhibit some oscillations. As $x_0 > 0$, i.e. $V_{\mathrm{c}} < V_0$, and for $x_{\max} > 0$, the variable x can never become negative, and the trap stays into a capturing state. On the contrary, if x_0 becomes negative, i.e. $V_{\mathrm{c}} > V_0$, x will oscillate between the values 0 and $x_{\max}$ with the period T defined in equation (2.7). This period diverges as x_0 becomes positive because no oscillations are possible. So we approximate the trap dynamics via an Ornstein–Uhlenbeck process [13]. Actually, a stochastic period arises from the noise effect in the domain $x_0 > 0$.

The general solution of equation (4.10) is

$$x(t) = x_0 + \mathrm{e}^{-t/\tau}\left(x_{\max} - x_0 + \int_0 \Lambda(s)\,\mathrm{e}^{s/\tau}\,\mathrm{d}s\right), \tag{4.12}$$

where the initial condition is $x(0) = x_{\max}$, i.e. $V(0) = V_{\max}$. The Fokker–Planck equation [14] describes the time evolution of the probability density function of x; it can be written as follows:

$$\partial_t c(x,t) = \frac{1}{\tau}\partial_x((x - x_0)\,c) + D\partial_x^2 c, \tag{4.13}$$

where
$$D = \frac{\phi D_{\mathrm{L}}}{(V_{\max} - V_{\mathrm{c}})^2}. \tag{4.14}$$

The dimension of D is s^{-1}. Here we take the diffusion coefficient for a bilipid: $D_{\mathrm{L}} = 10^{-11}\,\mathrm{m}^2\,\mathrm{s}^{-1}$ [15]. The initial condition at $t = 0$ is $c(x,0) = \delta(x - x_{\max})$, and the boundary conditions are $c(0,t) = c(\infty, t) = 0$. We focus on the system behaviour for $x = 0$. In fact, if $x = 0$ ($V = V_{\mathrm{c}}$), the value of the volume is instantaneously reset to $V_{\max}$. The probability flux $j(t)$ at $x = 0$ is

$$j(t) = D\,\partial_x c(x,t)|_{x=0}\,. \tag{4.15}$$

By integrating this flux over the whole temporal domain, we deduce the probability ϵ that the system escapes at $x = 0$:

$$\epsilon = \int_0^\infty j(t)\mathrm{d}t. \tag{4.16}$$

We note $\hat{c}(x,s)$ the Laplace transform of $c(x,\,t)$. By performing the Laplace transform of (4.13) and by imposing the initial boundary condition, we obtain

$$\begin{aligned} &-\delta(x - x_{\max}) + s\hat{c}(x,s) \\ &\quad = \frac{1}{\tau}\partial_x((x - x_0)\hat{c}(x,s)) + D\partial_x^2\hat{c}(x,s), \end{aligned} \tag{4.17}$$

The solution $\hat{c}$ of the earlier-mentioned equation allows us to compute the Laplace transform $\hat{j}(s)$ of the probability flux:

$$\hat{j}(s) = D\partial_x\hat{c}|_{x=0}. \tag{4.18}$$

Because $\hat{j}(s) = \int_0^\infty j(t)\,\mathrm{e}^{-st}\,\mathrm{d}t$, we deduce the following

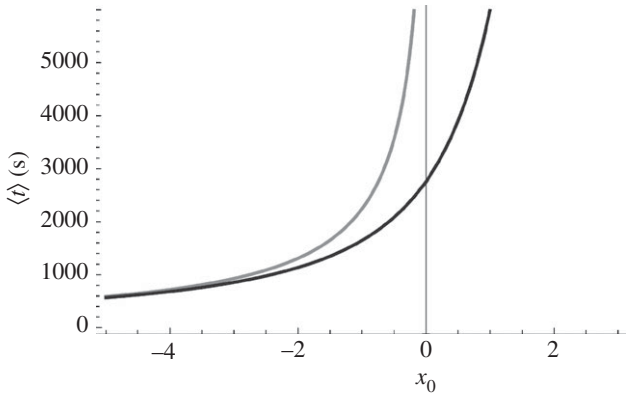

Figure 13. Average period of oscillation versus x_0. The grey curve represents the deterministic period (4.22). The black curve represents the average period for the stochastic system (4.21). As x_0 tends to minus infinity, we can neglect the influence of the noise, and the two curves join together. $D \sim 3.6 \times 10^{-4}$ s^{-1} and $\tau \sim 3232$ s.

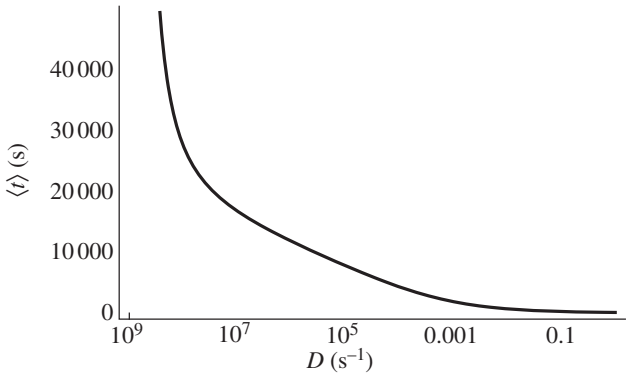

Figure 14. Average period of oscillation versus the noise intensity D in the excitable regime (region A). $x_0 = 0.0066$ and $\tau = 3232$ s.

Taylor expansion:

$$\hat{j}(s) = \int_0^\infty j(t)\mathrm{d}t - s\int_0^\infty tj(t)\mathrm{d}t = \epsilon(1 - s\langle t\rangle) + o(s^2). \tag{4.19}$$

As a consequence, a Taylor expansion for small s of the latter quantity permits us to identify the average first escape time

$$\langle t\rangle = \left.\frac{\partial_s \hat{j}(s)}{\hat{j}(s)}\right|_{s=0}, \tag{4.20}$$

which can be evaluated once $\hat{c}$ is known.

The computation of the probability flux is described in appendix B.

4.3. Computation of average escape time

We can evaluate the average first exit time $\langle t\rangle$ using (4.20):

$$\langle t\rangle = -\tau\left(\partial_z H_z\left(\frac{x_{\max} - x_0}{\sqrt{2D\tau}}\right) - \partial_z H_z\left(\frac{-x_0}{\sqrt{2D\tau}}\right)\right)\Bigg|_{z=0}, \tag{4.21}$$

where $H_z(y)$ is the Hermite polynomial of degree z. As shown in figure 13, for low noise, the stochastic period of the oscillations given by (4.21) tends to the deterministic period T_V (2.7). In terms of the variable x:

$$T_V = \tau\log\left(-\frac{x_{\max} - x_0}{x_0}\right). \tag{4.22}$$

As x_0 becomes negative, the system exhibits oscillations. In the simulation of the metronomic system (region D) displayed in figure 11, $x_0 = -0.2023$ and we find $T_V \sim 95$ min, which is in good agreement with [5] (from 45 min to several hours). In figure 13, we see that the fluctuations reduce the oscillation period.

In the excitable regime, x_0 is small. In figure 14, we can see that the noise extends the periodic behaviour for $x_0 > 0$. Unsurprisingly, an increasing noise intensity shortens the period.

5. CONCLUSION

The model is found to capture all the features of the mechanical system of *Utricularia* traps.

On the basis of simple mechanical ingredients, nonlinear elasticity and fluid coupling, the present analysis could be useful for other mechanical systems exhibiting oscillations, in the plant or animal kingdoms.

The precise quantification of all noise sources (physiological variations, fatigue, mechanism of pumping, variability in door elasticity or closure, etc.), is yet to be analysed, and opens perspective for future research.

APPENDIX A. STOCHASTIC VOLUME EQUATION

A.1. Statistical description of the membrane

Let us assume that the membrane may be described by a collection of N interconnected 'particles'. The positions of those 'particles' follow the Langevin equations that we write in the barycentric coordinates (for the sake of simplicity) as

$$\forall 1 \le j \le N, \partial_t \boldsymbol{r}_j = \frac{D_L}{k_b T}\boldsymbol{f}_j + \boldsymbol{\eta}_{bj}, \tag{A 1}$$

where $\boldsymbol{f}_j$ is the external force on the jth particle and where the Gaussian random drifts are defined by

$$\left.\begin{aligned} &\langle\, \boldsymbol{\eta}_{bj}(t)\rangle = \boldsymbol{0} \\ \text{and}\quad &\langle\, \boldsymbol{\eta}_{bj}(t)\, \boldsymbol{\eta}_{bj}(t')\rangle = 2D_L\delta(t - t'). \end{aligned}\right\} \tag{A 2}$$

The gyradius R_g of the membrane is defined by

$$R_g^2 = \frac{1}{N}\sum_j \boldsymbol{r}_j{}^2\,. \tag{A 3}$$

This is a measure of the statistical expansion of the membrane. That gyradius allows us to define the volume of gyration of the membrane as

$$V_g = \frac{4\pi}{3}(R_g^2)^{3/2} = \frac{4\pi}{3N^{3/2}}\left(\sum_j \boldsymbol{r}_j^2\right)^{3/2}, \tag{A 4}$$

which is the average statistical volume enclosed by the

membrane. Accordingly,

$$\partial_t V_{\mathrm{g}} = \frac{4\pi}{N^{3/2}} \left(\sum_j {\boldsymbol{r}_j}^2 \right)^{1/2} \left(\sum_j \boldsymbol{r}_j . \partial_t \boldsymbol{r}_j \right), \tag{A 5}$$

then

$$\partial_t V_{\mathrm{g}} = \frac{4\pi}{N} R_{\mathrm{g}} \left(\sum_j \boldsymbol{r}_j . \boldsymbol{\eta}_{bj} + \sum_j \frac{D_{\mathrm{L}}}{k_{\mathrm{b}} T} \boldsymbol{f}_j . \boldsymbol{r}_j \right). \tag{A 6}$$

A.2. Fluctuations near the resting volume

Normally, we expect the Gaussian noise to be negligible against the external forces. So we are interested only in the case where the sum of the external forces is about zero on each 'particle', that is when the second term in (A 6) tends to vanish. If we assume that we have small fluctuations, then we can approximate that all the r_j are near their initial values. Consequently, $\boldsymbol{r}_j . \boldsymbol{\eta}_{bj} \simeq r_j \, \boldsymbol{\eta}'_b$, where $\boldsymbol{\eta}'_b$ is the projection of a Gaussian random drift on a constant direction, so that

$$\left.\begin{aligned} \langle \boldsymbol{\eta}'_{bj}(t) \rangle &= 0 \\ \text{and} \qquad \langle \boldsymbol{\eta}'_{bj}(t) \boldsymbol{\eta}'_{bj} \rangle &= 2 D_{\mathrm{L}} \delta(t - t'). \end{aligned}\right\} \tag{A 7}$$

By the statistical summation of Gaussian random variables, we obtain

$$\frac{1}{N} \sum_j r_j \, \boldsymbol{\eta}'_{bj}(t) = R_{\mathrm{g}} \, \boldsymbol{\eta}'_b \tag{A 8}$$

where $\boldsymbol{\eta}'_b$ possesses the same properties than one of the $\boldsymbol{\eta}'_{bj}$. Finally, the evolution of the volume can be approximated by

$$\partial_t V_{\mathrm{g}} \simeq 4\pi \left(R_{\mathrm{g}}^2 \, \boldsymbol{\eta}'_b + R_{\mathrm{g}} \sum_j \frac{D_{\mathrm{L}}}{k_{\mathrm{b}} T} \boldsymbol{f}_j . \boldsymbol{r}_j \right). \tag{A 9}$$

The first (stochastic) term can be expressed as an overall Gaussian noise. Then the linearization of the second (deterministic) term near the resting volume $V_{\mathrm{g},0}$ shall mandatorily produce a first-order relaxation. This yields

$$\partial_t V_{\mathrm{g}} = \frac{1}{\tau} (V_{\mathrm{g},0} - V_{\mathrm{g}}) + \Lambda_{\mathrm{g}}(t), \tag{A 10}$$

where $\Lambda_{\mathrm{g}}(t)$ is a Gaussian volume drift with

$$\left.\begin{aligned} \langle \Lambda_{\mathrm{g}}(t) \rangle &= 0 \\ \text{and} \qquad \langle \Lambda_{\mathrm{g}}(t) \Lambda_{\mathrm{g}}(t') \rangle &= 2 S_{\mathrm{g}}^2 D_{\mathrm{L}} \delta(t - t'), \end{aligned}\right\} \tag{A 11}$$

where $S_{\mathrm{g}} = 4\pi R_{\mathrm{g}}^2$ is by definition the gyration surface.

A.3. Application to Utricularia

The equation for the trap may be deduced by

$$\partial_t V_m \approx \frac{1}{\tau} (V_{m,0} - V_m) + \underbrace{\frac{V_m}{V_{\mathrm{g}}} \Lambda_{\mathrm{g}}(t)}_{\Lambda_m(t)} \tag{A 12}$$

with

$$\left.\begin{aligned} \langle \Lambda_m(t) \rangle &= 0 \\ \text{and} \quad \langle \Lambda_m(t) \Lambda_m(t') \rangle &= 2 \frac{V_m^2}{V_{\mathrm{g}}^2} S_{\mathrm{g}}^2 D_{\mathrm{L}} \delta(t - t'), \end{aligned}\right\} \tag{A 13}$$

and

$$\langle \Lambda_m(t) \Lambda_m(t') \rangle = 2 \phi D_{\mathrm{L}} \delta(t - t'), \tag{A 14}$$

where

$$\phi = \left(\frac{9 V_m^2}{R_{\mathrm{g}}^2} \right). \tag{A 15}$$

Taking into account the cylindrical geometry

$$R_{\mathrm{g}}^2 = \frac{\Gamma_{\mathrm{g}}^2}{S_{\mathrm{m}}}, \tag{A 16}$$

with

$$\Gamma_{\mathrm{g}}^2 = 2\pi \left[2 \int_0^{L/2} \left(r + \frac{e}{2} \right)^2 r \, \mathrm{d}r + L \int_0^{e/2} \left(\frac{L}{2} + z \right)^2 \mathrm{d}z \right], \tag{A 17}$$

we can compute

$$\phi = \frac{9 V_m^2 S_{\mathrm{m}}}{\Gamma_p^2} = \frac{27 e^2 \pi^2 L^4 (L + 2e)}{2(3L + 2e)(L^2 + 6eL + 2e^2)}. \tag{A 18}$$

This crude modelling allows us to connect a microscopic particular diffusion coefficient D_{L} to a macroscopic volume diffusion coefficient $2\phi D_{\mathrm{L}}$.

APPENDIX B. COMPUTATION OF THE PROBABILITY FLUX

We first solve (4.17). The presence of the dirac function localized at $x = x_{\max}$ suggests to consider two intervals. On the first interval $[0, x_{\max}]$, we compute the solution $\hat{c}_a(x, s)$, whereas we note $\hat{c}_b(x, s)$ the solution on the interval $[x_{\max}, \infty[$, such that we have to solve the following equation:

$$\begin{aligned} s \hat{c}_{a,b}(x, s) = \frac{1}{\tau} \partial_x ((x - x_0) \, \hat{c}_{a,b}(x, s)) \\ + D \partial_x^2 \, \hat{c}_{a,b}(x, s). \end{aligned} \tag{B 1}$$

We find the asymptotic solution:

$$\hat{c}^{\infty}_{a,b}(x, s) = \mathrm{e}^{-(x - x_0)^2 / 2D\tau}. \tag{B 2}$$

The sought solutions of (B 1) are written:

$$\hat{c}_i = i_1(s) f_1(x, s) + i_2(s) f_2(x, s), \tag{B 3}$$

$$f_1(x, s) = \mathrm{e}^{-(x - x_0)^2 / 2D\tau} H_{-s\tau} \left(\frac{x - x_0}{2D\tau} \right) \tag{B 4}$$

and

$$f_2(x, s) = \mathrm{e}^{-(x - x_0)^2 / 2D\tau} \, {}_1F_1 \left(\frac{s\tau}{2}; \frac{1}{2}; - \frac{(x - x_0)^2}{2D\tau} \right). \tag{B 5}$$

The index i stands for a,b. $H_n(z)$ is the Hermite polynomial of degree n and ${}_1F_1$ $(a';b';z)$ is the Kummer confluent hypergeometric function. Note the similarity of the function f_1 with the wave function of the quantum harmonic oscillator. The function $f_2(x,s)$ behaves as $1/x$, as x tends to infinity, and this slow convergence to zero imposes that $b_2 = 0$, because we aim in deriving a finite density probability. As consequence we have

three unknowns ($a_{1,2}$ and b_1) for the three boundary conditions:

$$\hat{c}_a(0,s) = 0, \tag{B 6}$$

$$\hat{c}_a(x_{\max},s) = \hat{c}_b(x_{\max},s) \tag{B 7}$$

and

$$\hat{c}'_b(x_{\max},s) - \hat{c}'_a(x_{\max},s) = -\frac{1}{D}. \tag{B 8}$$

The last condition is the consequence of the presence of the dirac function located at $x = x_{\max}$. The inversion of system (B 6)–(B 8) gives

$$a_1 = \frac{f_1(x_{\max},s) f_2(s,0)}{D f_1(s,0) w(x_{\max},s)}, \tag{B 9}$$

$$a_2 = -\frac{f_1(x_{\max},s)}{D w(x_{\max},s)} \tag{B 10}$$

and

$$b_1 = \frac{f_1(x_{\max},s) f_2(s,0) - f_1(s,0) f_2(x_{\max},s)}{D f_1(s,0) w(x_{\max},s)}, \tag{B 11}$$

where $w(x,s) = f_2(x,s)\partial_x f_1(x,s) - f_1(x,s)\partial_x f_2(x,s)$ is the Wronskian of the equation (B 1). It obeys the equation

$$D\partial_x w + \frac{1}{\tau}(x - x_0) w = 0, \tag{B 12}$$

which has as a solution $w(x,s) = A e^{-(x-x_0)^2/2D\tau}$. Consequently, we deduce that the probability flux defined in (4.18) takes the following form:

$$\hat{j} = \frac{f_1(x_{\max},s) w(0,s)}{f_1(0,s) w(x_{\max},s)}. \tag{B 13}$$

Furthermore, we can compute the probability ϵ that the system escapes at $x = 0$ is 1 because

$$\epsilon = \frac{f_1(x_{\max},0) w(0,0)}{f_1(0,0) w(x_{\max},0)}. \tag{B 14}$$

and $H_0(z) = 1$. This means that a noisy trap shall always fire.

REFERENCES

1 Sydenham, P. H. & Findlay, G. P. 1975 Transport of solutes and warter by resetting bladders of *Utricularia*. *Aust. J. Plant Physiol.* **2**, 335–351.
2 Juniper, B. E., Robins, R. J. & Joel, D. M. 1989 *The carnivorous plants*. London, UK: Academic Press.
3 Vincent, O., Weißkopf, C., Poppinga, S., Masselter, T., Speck, T., Joyeux, M., Quilliet, C. & Marmottant, P. 2011 Ultra-fast underwater suction traps. *Proc. R. Soc. B* **278**, 2909–2914. (doi:10.1098/rspb.2010.2292)
4 Joyeux, M., Vincent, O. & Marmottant, P. 2011 Mechanical model of the ultrafast underwater trap of *Utricularia*. *Phys. Rev. E* **83**, 021911. (doi:10.1103/PhysRevE.83.021911)
5 Vincent, O., Roditchev, I. & Marmottant, P. 2011 Spontaneous firings of carnivorous aquatic *Utricularia* traps: temporal patterns and mechanical oscillations. *PLoS ONE* **6**, e20205.
6 Burkitt, A. N. 2006 A review of the integrate-and-fire neuron model: I. Homogeneous synaptic input. *Biol. Cybern.* **95**, 1–19. (doi:10.1007/s00422-006-0068-6)
7 Frensch, J. & Steudle, E. 1989 Axial and radial hydraulic resistance to roots of maize (*Zea mays* L.). *Plant Physiol.* **91**, 719–726. (doi:10.1104/pp.91.2.719)
8 Forterre, Y., Skotheim, J. M., Dumais, J. & Mahadevan, L. 2005 How the Venus flytrap snaps. *Nature* **433**, 421–425. (doi:10.1038/nature03185)
9 Kuramoto, Y. 2003 *Chemical oscillations, waves, and turbulence*. New York, NY: Dover Books.
10 Lamb, H. 1982 *Hydrodynamics*. Cambridge, UK: Cambridge University press.
11 Landau, L. D. & Lifshitz, E. M. 1987 *Fluid mechanics*. Oxford, UK: Pergamon Press.
12 Landau, L. D. & Lifshitz, E. M. 1987 *Theory of elasticity*. Oxford, UK: Pergamon Press.
13 Uhlenbeck, G. E. & Ornstein, L. S. 1930 On the theory of Brownian motion. *Phys. Rev.* **36**, 823–841. (doi:10.1103/PhysRev.36.823)
14 Van Kampen, N. G. 1981 *Stochastic processes in physics and chemistry*. Amsterdam, The Netherlands: North-Holland Publishing Co.
15 Eriksson, P. O. & Lindblom, G. 1993 Lipid and water diffusion in bicontinuous cubic phases measured by NMR. *Biophys. J.* **64**, 129–136. (doi:10.1016/S0006-3495(93)81347-X)